Chemistry & Biology
Article

Characterization of Bioactive Cell Penetrating Peptides from Human Cytochrome *c*: Protein Mimicry and the Development of a Novel Apoptogenic Agent

Sarah Jones,[1,*] Tina Holm,[2] Imre Mäger,[3] Ülo Langel,[2,3] and John Howl[1,*]
[1]Molecular Pharmacology Research Group, Research Institute in Healthcare Science, School of Applied Sciences, University of Wolverhampton, Wulfruna Street, Wolverhampton, WV1 1SB, UK
[2]Department of Neurochemistry, Stockholm University, S. Arrheniusv 21A, Stockholm SE-10691, Sweden
[3]Laboratory of Molecular Biotechnology, Institute of Technology, Tartu University, Nooruse 1, 50411 Tartu, Estonia
*Correspondence: s.jones4@wlv.ac.uk (S.J.), j.howl@wlv.ac.uk (J.H.)
DOI 10.1016/j.chembiol.2010.05.018

SUMMARY

Cell penetrating peptides (CPPs) with intrinsic biological activities offer a novel strategy for the modulation of intracellular events. QSAR analysis identified CPPs within human cytochrome *c*. Two such sequences, Cyt $c^{77–101}$ and Cyt $c^{86–101}$, induced tumor cell apoptosis, thus mimicking the role of Cyt *c* as a key regulator of programmed cell death. Quantitative analyses confirmed that Cyt $c^{77–101}$ is an extremely efficient CPP. Thus, Cyt $c^{77–101}$ was selected for modification to incorporate target-specific peptidyl motifs. Chimeric N-terminal extension with a target mimetic of FG nucleoporins significantly enhanced the apoptogenic potency of Cyt $c^{77–101}$ to a concentration readily achievable in vivo. Moreover, this construct, Nup153-Cyt *c*, facilitates the dramatic redistribution of nuclear pore complex proteins and thus propounds the nuclear pore complex as a novel target for the therapeutic induction of apoptosis.

INTRODUCTION

Protein interfaces facilitate molecular recognition events that influence many aspects of cellular physiology and pathology. Mimetic peptides that include sequences derived from protein interfaces and other functional domains can potentially make multiple contacts with their target proteins. Subsequently, these binding events may initiate a selective modulatory action akin to the parent signal transduction protein. For example, a decapeptide mimetic of the carboxyl terminus of $G_i3\alpha$ (KNNLKECGLY, $G_i3\alpha^{346–355}$), a component of heterotrimeric G proteins, promotes the dual phosphorylation of p42/p44 MAP kinases when translocated into cells by the cell penetrating peptide (CPP) transportan-10 (Jones et al., 2005). Related studies further identified induction of mast cell secretion following intracellular delivery of peptides derived from protein kinase C and the C-terminal juxtamembrane region of the central cannabinoid (CB_1) receptor (Howl et al., 2003).

Such results clearly demonstrate that small- to medium-sized peptides, delivered to an appropriate intracellular compartment, can modulate common signal transduction pathways that control both acute and chronic features of cellular physiology and pathology. Since corrupted signaling events often underpin many diseased states such as cancer, these studies also exemplify the potential of mimetic peptides to target and specifically modulate novel therapeutic loci that underlie cellular proliferation, apoptosis and differentiation. To date, several exemplary studies have propounded the utility of mimetic peptides for such purposes and among which include, suppression of malignant cells in vivo by the intracellular delivery of a proteolytically resistant *retro-inverso* mimetic corresponding to the C-terminal of the tumor suppressor p53 (Snyder et al., 2004) and abrogation of breast cancer cellular proliferation by a cell-permeable 22 amino acid peptide derived from the N-terminal of the tumor suppressor protein p14ARF (Johansson et al., 2008). Similarly, an octameric mimetic of the N-terminal of Smac/Diablo, when fused to the CPP penetratin, binds to inhibitor of apoptosis proteins (IAPs) with a consequential liberation of sequestered caspases and thus enhances the induction of apoptosis and antiproliferative effects of antineoplastic pharmacotherapeutics (Arnt et al., 2002); continued studies have strengthened the application of this peptide in vivo (Fulda et al., 2002).

The past decade has witnessed an escalating interest in the therapeutic applications of CPPs (Derossi et al., 1994). Alternatively designated protein transduction domains, CPPs, have demonstrated utility as vectors for the highly efficient delivery of bioactive cargoes into the intracellular milieu (Langel, 2007). Derived from either endogenous proteins (e.g., penetratins; Derossi et al., 1994) or entirely synthetic in nature (e.g., Model Amphipathic Petide (MAP) sequences; Lindgren et al., 2000), a vast majority of CPPs are polycationic or amphipathic and so comprise multiple Arg and/or Lys residues that confer cell penetrating properties. The majority of studies to date have employed sychnologically organized combinations (Portoghese, 1989) of a cargo (message) and a CPP (address) joined as a tandem construct. Bioactive cargoes have included peptides, proteins, cytotoxins, and oligonucleotides including short interfering RNA and peptide nucleic acids (Langel, 2007; Schwarze and Dowdy, 2000). Moreover, CPPs also improve the intracellular delivery of larger moieties such as liposomes when assembled as noncovalent complexes (Tseng et al., 2002).

More recently, a QSAR-based algorithm has been developed to predict cryptic polycationic CPP motifs within the primary sequences of proteins (Hällbrink et al., 2005). Moreover, Arg,

A

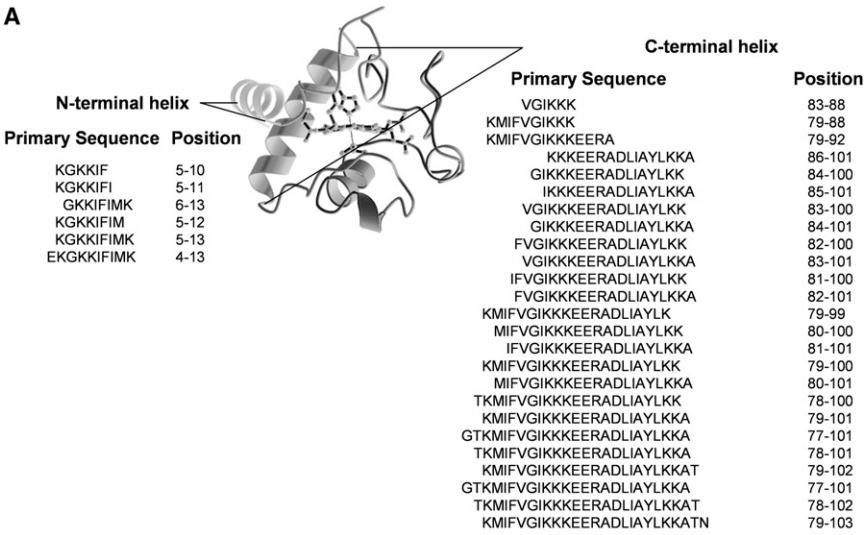

Primary Sequence	Position
KGKKIF	5-10
KGKKIFI	5-11
GKKIFIMK	6-13
KGKKIFIM	5-12
KGKKIFIMK	5-13
EKGKKIFIMK	4-13

Primary Sequence	Position
VGIKKK	83-88
KMIFVGIKKK	79-88
KMIFVGIKKKEERA	79-92
KKKEERADLIAYLKKA	86-101
GIKKKEERADLIAYLKK	84-100
IKKKEERADLIAYLKKA	85-101
VGIKKKEERADLIAYLKK	83-100
GIKKKEERADLIAYLKKA	84-101
FVGIKKKEERADLIAYLKK	82-100
VGIKKKEERADLIAYLKKA	83-101
IFVGIKKKEERADLIAYLKK	81-100
FVGIKKKEERADLIAYLKKA	82-101
KMIFVGIKKKEERADLIAYLK	79-99
MIFVGIKKKEERADLIAYLKK	80-100
IFVGIKKKEERADLIAYLKKA	81-101
KMIFVGIKKKEERADLIAYLKK	79-100
MIFVGIKKKEERADLIAYLKKA	80-101
TKMIFVGIKKKEERADLIAYLKK	78-100
KMIFVGIKKKEERADLIAYLKKA	79-101
GTKMIFVGIKKKEERADLIAYLKKA	77-101
TKMIFVGIKKKEERADLIAYLKKA	78-101
KMIFVGIKKKEERADLIAYLKKAT	79-102
GTKMIFVGIKKKEERADLIAYLKKA	77-101
TKMIFVGIKKKEERADLIAYLKKAT	78-102
KMIFVGIKKKEERADLIAYLKKATN	79-103

B

Peptide Sequence	Abbreviation
H-GTKMIFVGIKKKEERADLIAYLKKA-NH_2	Cyt $c^{77\text{-}101}$
H-KKKEERADLIAYLKKA-NH_2	Cyt $c^{86\text{-}101}$
H-KMIFVGIKKKEERA-NH_2	Cyt $c^{79\text{-}92}$
H-KMIFVGIKKK-NH_2	Cyt $c^{79\text{-}88}$
H-EKGKKIFIMK-NH_2	Cyt $c^{4\text{-}13}$
H-KGKKIFIMK-NH_2	Cyt $c^{5\text{-}13}$
H-INLKKLAKL(Aib)KKIL-NH_2	mitP
H-RQIKIWFQNRRMKWKK-NH_2	penetratin
H-MVTVLFRRLRIRRACGPPRVRV-NH_2	M918
CH_3CO-NFKFGLSS-NH_2	Nup153 $^{980\text{-}987}$
CH_3CO-NFKFGLSS(Ahx)GTKMIFVGIKKKEERADLIAYLKKA-NH_2 (*Ac*-Nup153$^{980\text{-}987}$(Ahx)Cyt $c^{77\text{-}101}$)	Nup153-Cyt *c*
CH_3CO-GFSNSFKLN(Ahx)GTKMIFVGIKKKEERADLIAYLKKA-NH_2 (*Ac-scr*Nup153$^{980\text{-}987}$(Ahx)Cyt $c^{77\text{-}101}$)	*scr*Nup153-Cyt *c*
CH_3CO-NFKFGLSS(Ahx)RQIKIWFQNRRMKWKK-NH_2	Nup153-penetratin
H-CNFKFGLSSK(N$^{\varepsilon}$-5,6-carboxy-flourescein)-NH_2 | *H*-CMVTVLFRRLRIRRACGPPRVRV-NH_2	*Fluo*-Nup153-M918

Figure 1. Cryptic CPP Sequences of Cyt *c*

(A) Quaternary structure of Cyt *c* and the restricted distribution of cryptic CPP sequences. Highly probable CPPs are located in the amino and carboxyl termini.

(B) Peptide sequences and abbreviations of cryptic CPP and other peptides used in this study. Vertical lines indicate a disulphide bridge.

and less commonly Lys, is often distributed at the site of protein interfaces. Hence, we considered it very likely that some cryptic CPP sequences within the primary sequences of key signaling proteins should have intrinsic biological activity. Moreover, the identification of proteomimetic CPPs, in which multiple pharmacophores for cellular penetration and biological activities are presumed to be discontinuously (rhegnylogically) organized within the primary sequence (Portoghese, 1989), would represent a new class of biological agent.

The major aim of this study was to employ human cytochrome *c* (Cyt *c*) as a prediction template to enable the identification of CPPs that can mimic the trafficking events and apoptogenic activity of the native protein. This investigation also provided a rigorous assessment of the utility of the prediction algorithm to identify new CPP sequences. Having identified a range of CPPs, one peptide, with an enhanced propensity for cellular penetration, was selected for further development as a chimeric apoptogenic agent that targets components of the nuclear pore complex (NPC), specifically the FG nucleoporins (FG Nups), as a novel therapeutic strategy. Characterized by multiple FXFG repeat sequences, FG Nups regulate import and export between the cytoplasm and the nucleus. Nup153 was the target protein of choice since it is one of the most characterized of the FG Nups and assumes roles in nuclear import and the regulation of pore selectivity, nuclear basket formation, nuclear pore complex anchoring and nuclear envelope breakdown (Walther et al., 2001; Prunuske et al., 2006).

RESULTS

Human Cyt *c* as a CPP Prediction Template: Distribution of Predicted CPPs within the Human Cyt *c* Protein

Human Cyt *c* (Figure 1A), a highly conserved 10 aa protein, has well-documented dual roles in mitochondrial electron transport and intrinsic apoptotic events (Jiang and Wang, 2004). This study was, therefore, primarily designed to address the fundamental question of whether cell penetrating fragments of Cyt *c* could mimic the apoptogenic activity of the native protein. Using the QSAR-based prediction algorithm (Hällbrink et al., 2005) to delineate putative CPPs within the primary sequences of Cyt *c*, peptides were ranked from 1 (lowest probability) to 3 (highest probability). We chose to focus our efforts entirely on *highly probable* CPP sequences (Figure 1A). Furthermore, an extended range of Cyt *c*-derived peptides was included in these studies to provide both a more rigorous assessment of this general strategy and to supplement previous investigations limited to Cyt $c^{77\text{–}101}$ and Cyt $c^{86\text{–}101}$ (Howl and Jones, 2008) (Figure 1B).

As indicated in Figure 1A, QSAR analysis of human Cyt *c* identified 31 highly probable CPPs of which 25 were derived from the larger carboxyl-terminal helix. Predicted CPPs within the size range of 5–25 aa were entirely restricted in topological distribution to the two major helical domains, closely associated

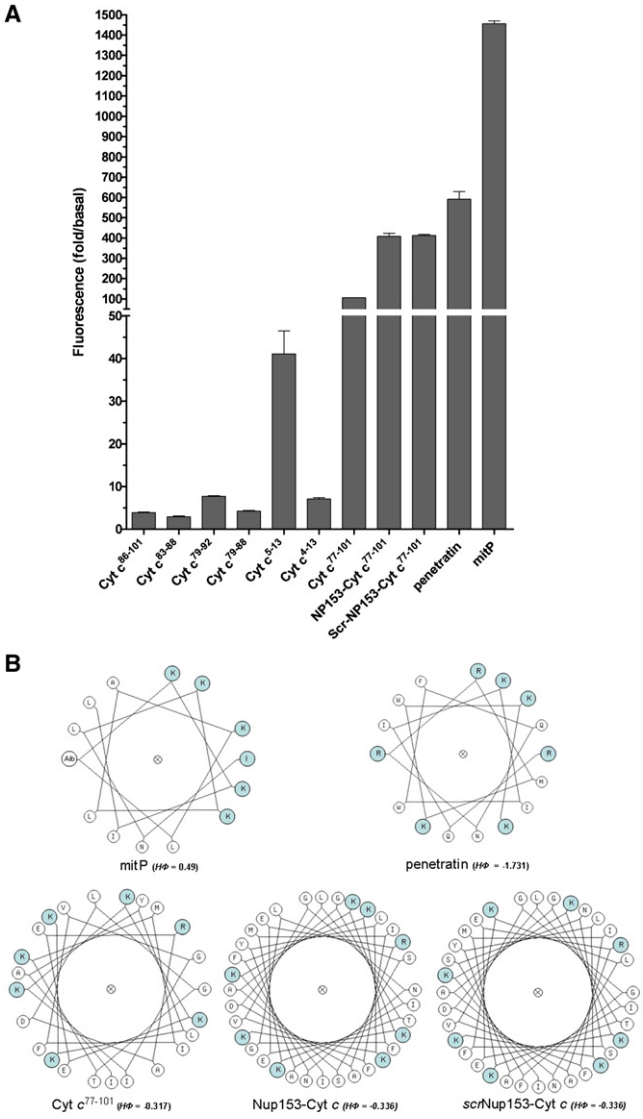

Figure 2. Translocation Efficacies and Predictions of Secondary Structure of Cyt *c*-Derived CPPs

(A) Translocation efficacies. U373MG cells were incubated with fluorescently labeled peptides (5 μM) for 1 hr at 37°C. Cell lysates were analyzed by fluorescence spectroscopy and results expressed as fold/basal fluorescence from three experiments performed in triplicate.

(B) Helical wheel projections of highly penetrant peptides derived from Cyt *c*. The well-characterized CPP penetratin and mitP have been included for comparison. Projections show the distribution of cationic charge (shaded amino acids). Diagrams were produced using the helical wheel interactive Java Applet (http://kael.net/helical.htm). X denotes the known helix promoter α- aminoisobuytyric acid (Aib).

in the mature protein, that comprise the amino and carboxyl termini of the protein (Figure 1A).

Comparative Translocation Efficacies of Cyt *c*-Derived CPP

As indicated in Figure 2A, CPPs derived from Cyt *c* exhibited a large dynamic range of translocation efficacies. As previously reported (Howl and Jones, 2008), and despite the relatively low translocation efficacy indicated here (Figure 2A), Cyt $c^{86–101}$ can be observed specifically located within the nucleus of U373MG cells (Table 1). These comparative data further indicate that, of all Cyt *c*-derived CPPs included in this study, Cyt $c^{77–101}$ is a very efficient CPP (105.9 ± 0.42-fold uptake).

The well-characterized CPP penetratin was also included in this quantitative analysis of intracellular uptake and demonstrated a 591.3 ± 37.52-fold uptake. Comparative investigations also included the mitochondriotoxic CPP mitoparan (mitP) (Jones et al., 2008) that, as demonstrated in Figure 2A, gave a 1455.8 ± 13.8-fold uptake. MitP is a peptide analog of the α−helical amphipathic tetradecapeptide mastoparan and was designed to incorporate sequence permutations that enhanced amphipathicity by introducing additional cationic charge within the hydrophilic face of mastoparan (Jones and Howl, 2004). As indicated by predictions in secondary structure (Figure 2B), mitP presents six positive charges, 5 lysyl ε-amino groups, and the amino terminus of Ile, within its hydrophilic face. Given that mitP also demonstrates an enhanced propensity for cellular penetration and that amphipathic sequences are more likely to be cell penetrant, predictions in secondary structure were carried out to ascertain whether other highly penetrant sequences in this study shared the same biochemical traits. Figure 2B demonstrates that while mitP clearly shows a marked delineation between its hydrophobic and hydrophilic faces, such a patent dichotomy is not apparent within other designated highly penetrant cationic CPP.

Biological Profiles of Cryptic CPP Derived from Cyt *c*

Having identified a range of CPPs, and given that Cyt *c* is a key regulator of programmed cell death, each sequence was evaluated for its ability to induce apoptosis alongside establishment of intracellular distribution. U373MG astrocytoma was used as a model cell line since it is well characterized and used in our laboratory to examine apoptotic events. Both Cyt $c^{77–101}$ and Cyt $c^{86–101}$ specifically induced apoptosis, as was confirmed by TUNEL assay in situ and activation of caspase-3 (Table 1), though changes in cellular viability measured by MTT conversion demonstrated only moderate potencies for Cyt $c^{86–101}$ and Cyt $c^{77–101}$, with LD_{50} values of 51.42 and 80.63 μM, respectively. Other cryptic peptides presented in Table 1 were excluded from further study owing to their inability to reduce cellular viability at physiologically acceptable concentrations.

Live confocal cell imaging indicated that Cyt $c^{77–101}$ and the shorter homolog Cyt $c^{86–101}$ translocated U373MG plasma membranes to differentially accumulate in extranuclear or nuclear compartments, respectively (Table 1) (Howl and Jones, 2008). More specifically, quantitative colocalization analyses demonstrated that Cyt $c^{77–101}$ strongly colocalized with the endoplasmic reticulum (ER) and gave a colocalization coefficient of 0.996 ± 0.002.

Selection of Nup153$^{980–987}$ As a Nuclear Pore-Targeting Motif

The highly cell penetrant yet moderately apoptogenic peptide Cyt $c^{77–101}$ was selected for further development as a chimeric apoptogenic agent. This chimeric strategy was largely pursued in the light of our recent developments with the mitochondriotoxic CPP mitP and its highly potent target-selective analogs (Jones

Table 1. Biological Profiles of CPP Derived from Cyt *c*

Peptide	LD_{50}	Intracellular Target	Apoptosis
Cyt $c^{86–101}$	51.42 μM	Nucleus	TUNEL positive Caspase-3 positive
Cyt $c^{77–101}$	80.63 μM	Endoplasmic reticulum	TUNEL positive Caspase-3 positive
Nup153-Cyt $c^{77–101}$	0.73 μM	Perinuclear	TUNEL positive Caspase-3 positive
*scr*Nup153-Cyt $c^{77–101}$	Not toxic	Cytoplasmic	Not toxic
Cyt $c^{79–92}$	>200 μM	Discontinued from this study due to their low translocation efficacies and inability to induce apoptosis	
Cyt $c^{79–88}$	>200 μM		
Cyt $c^{4–13}$	>200 μM		
Cyt $c^{5–13}$	>200 μM		

LD_{50} values represent the concentration of peptides required to induce apoptotic death of 50% of cultured U373MG cells. The intracellular target was determined by confocal microscopy of living cells and reports the propensity of different peptides to accumulate in various intracellular compartments. Where indicated, apoptosis has been confirmed by a combination of both TUNEL staining and caspase-3 activity.

et al., 2008). Thus, the overriding objective of this strategy was to enhance cytotoxicity and/or develop target-selective drug delivery vectors that combined both an apoptogenic CPP and a bioactive peptidyl motif. The apoptogenic potency of Cyt $c^{77–101}$ was most significantly enhanced by chimeric N-terminal extension with a sequence derived from the C-terminal of nucleoporin 153 (Nup153) (Figure 1B). The nonapeptide sequence $Nup153^{980–987}$ (NNFKFGLSS) contains the common tetrameric FXFG repeat that, in approximately one-third of nucleoporin proteins, mediates binding to transport receptors including importin β (Bednenko et al., 2003). Sequence design was also based on there being 15 FXFG repeat sequences throughout the Nup153 protein, 4 of which are FKFG, while numerous viscinal serines appear throughout.

We included this sequence, acetylated at the amino terminus to inhibit proteolysis, as a sychnologically organized amino-terminal extension of Cyt $c^{77–101}$ in the chimeric construct *Ac*-$Nup153^{980–987}$(Ahx)Cyt $c^{77–101}$ (Nup153-Cyt *c*) (Figure 1B). A similar construct with a scrambled Nup153 sequence (*scr*Nup153-Cyt *c*) (Figure 1B) was also included in cytotoxicity, translocation, and subcellular localization studies to confirm the specific bioactivity of the Nup153-derived FXFG-containing nonapeptide.

Characterization of Nup153-Cyt *c* As a Potent Apotogenic Chimera

N-terminal extension of Cyt $c^{77–101}$ with $Nup153^{980–987}$ significantly enhanced the cytotoxic potency of Cyt $c^{77–101}$. Thus, the chimeric construct Nup153-Cyt *c* induced apoptosis of U373MG astrocytoma with an LD_{50} of 0.73 μM, a concentration readily achieved in vivo, whereas the scrambled sequence *scr*Nup153-Cyt *c* (*Ac*-GFSNSFKLN(Ahx)Cyt$c^{77–101}$) and $Nup153^{980–987}$ alone were inactive (Figure 3A; Table 1). Apoptosis was confirmed as the mechanism of cell death and was demonstrated by the peptide's ability to activate caspase-3 and induce internucleosomal DNA fragmentation (Figures 3B and 3C). Furthermore, the translocation efficacies of both Nup153-Cyt *c* (408.2 ± 15.58-fold) and the biologically inactive scrambled construct *scr*Nup153-Cyt *c* (412.5 ± 5.20-fold) were enhanced compared to the native peptide Cyt $c^{77–101}$ (105.9 ± 0.42-fold) (Figure 2A). These data therefore suggest specificity of action for an intracelluar target by Nup153-Cyt *c* in the orchestration of apoptosis.

Nup153-Cyt *c* As a Novel Apoptogenic CPP and Its Mechanism of Action

To decipher the mechanism by which Nup153-Cyt *c* induced apoptotic events, $Nup153^{980–987}$ was translocated into U373MG cells by the inert CPP M918 as a fluorescein-conjugated disulphide-linked cargo *H*-CNFKGLSSK(N^{ε}-5,6-carboxyfluorescein)-NH_2 (*Fluo*-$Nup153^{980–987}$) (Figure 1B). *Fluo*-$Nup153^{980–987}$ demonstrated a distinct accumulation around the nuclear periphery (Figure 4A). Complementary studies were performed using the rhodamine-labeled chimeric structures *Rho*-Nup153-Cyt *c* and the control peptide *Rho-scr*Nup153-Cyt *c*. Confocal live cell imaging indicated that *Rho*-Nup153-Cyt *c* assumed a predominant perinuclear localization after 45 min of administration, whereas *Rho-scr*Nup153-Cyt *c* displayed a more generalized cytoplasmic distribution at a similar time point (Figure 4B). To further refine these early events, U373MG cells were treated with either *Rho*-Nup153-Cyt *c* or *Rho-scr*Nup153-Cyt *c* for 45 min and the nucleoporin protein Nup153 detected by immunostaining (Figure 4B). Quantitative colocalization analysis demonstrated that *Rho*-Nup153-Cyt *c* assumed a strong colocalization with Nup153 (*coloc* coefficient = 0.93 ± 0.024) compared with the diffusely distributed scrambled chimera (*coloc* coefficient = 0.157 ± 0.031) ($p < 0.0001$, unpaired *t* test, two-tailed).

Given the subcellular localizations of *Fluo*-$Nup153^{980–987}$ and *Rho*-Nup153-Cyt *c*, additional studies were performed to establish whether intracellular Nup153-Cyt *c* directly modulated the functional utility of the nuclear pore complex. Later events at 4 hr, analyzed using indirect immunofluorescence, demonstrated that Nup153-Cyt *c* facilitated the dramatic redistribution of the NPC protein Nup153 from the nuclear periphery to the nucleoplasm and cytoplasm (Figure 4D). Moreover, this relocation phenomenon was similarly observed in the presence of the pan-caspase inhibitor Q-VD-OPh and indicates that the redistribution of Nup153 in Nup153-Cyt *c*-treated cells is not a downstream consequence of caspase activation (Figure 4D).

Significantly, the intracellular delivery of $Nup153^{980–987}$, using either of the inert CPPs penetratin or M918, induced only moderate reductions in cellular viability (Figure 5) indicating that the apoptogenic properties of the chimeric peptide Nup153-Cyt *c* may in part be attributable to the peptide targeting additional intracellular sites, besides that of the nuclear pore complex. In light of these findings and given that the parent peptide Cyt $c^{77–101}$ demonstrates a strong propensity for colocalization (*coloc* coefficient = 0.996 ± 0.002) with the ER (Table 1), quantitative colocalization analysis with ER was performed with both *Rho*-Nup153-Cyt *c* and its scrambled analog. Both peptides gave a considerably low level of colocalization with *coloc* coefficients of 0.287 ± 0.065 and 0.354 ± 0.063, respectively. Thus, the enhanced apoptogenic potency demonstrated by Nup153-Cyt *c* may not be attributed to interaction with the ER. This line of investigation was pursued in the light of recent reports that native Cyt *c* binds inositol 1,4,5-trisphosphate

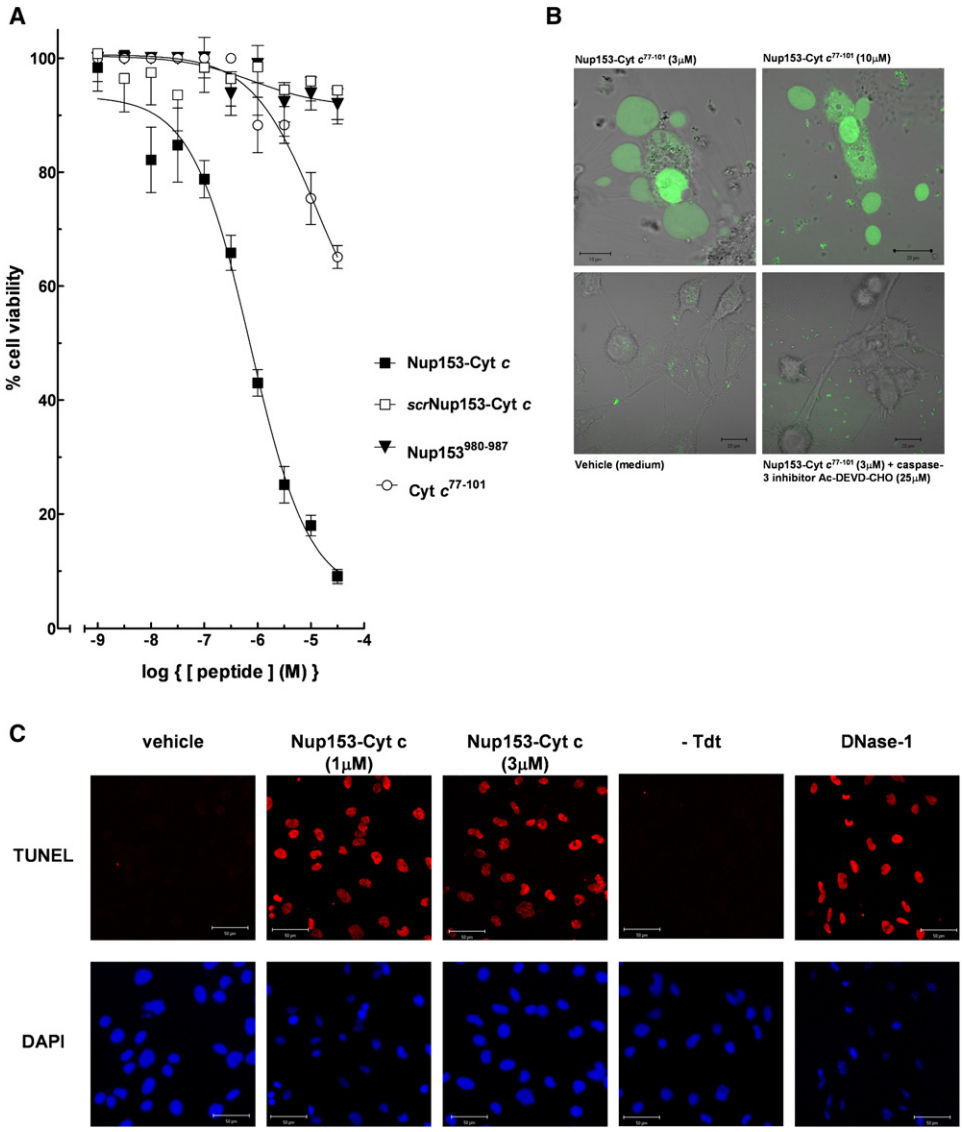

Figure 3. Characterization of Nup153-Cyt *c* as a Potent Apoptogenic Chimera

(A) N-terminal extension of Cyt $c^{77–101}$ with Nup153$^{980–987}$ significantly enhances the cytotoxic potency of Cyt $c^{77–101}$, while Nup153$^{980–987}$ and the scrambled sequence chimera *scr*Nup153-Cyt *c* are inactive. U373MG cells were exposed to increasing concentrations of peptides (0.001–30 μM) for 24 hr. Cell viability was measured by MTT conversion and expressed as a percentage of those cells treated with vehicle (medium) alone. Data points are mean ± SEM from three experiments performed in sextruplicate.

(B) Nup153-Cyt *c* induces apoptosis of U373MG astrocytoma as confirmed by activation of caspase-3. U373MG cells were treated with Nup153-Cyt *c* at the concentrations indicated for 4 hr. DEVD-NucView 488 caspase-3 substrate (Biotum, Inc.) was added at a final concentration of 5 μM for a further 30 min and cells were viewed by confocal live cell imaging. The cell permeable construct DEVD-NucViewTM 488 caspase-3 substrate consists of a functional high affinity DNA-binding dye that is rendered inert by the highly negatively charged DEVD peptide substrate. Upon activation of caspase-3, the substrate is cleaved to release a functional DNA dye that subsequently migrates to the nucleus. Green fluorescence seen in the nuclei of Nup153-Cyt *c*-treated cells indicates activation of caspase-3, compared with cells treated with medium alone (vehicle) or treated cells incubated with the caspase-3 inhibitor Ac-DEVD-CHO (25 μM).

(C) Nup153-Cyt *c* induces apoptosis of U373MG astrocytoma as confirmed by nuclear DNA fragmentation. U373MG cells were treated with Nup153-Cyt *c*, at the concentrations indicated or with vehicle alone for 18 hr. Cells were fixed in 4% (w/v) formaldehyde and permeabilized with 0.1% (v/v) Triton X-100. Nuclear DNA fragmentation was detected by TUNEL in situ cell detection assay TMR red (Roche), and cells were counterstained with DAPI to visualize nuclear DNA. Representative examples are shown. The appearance of TMR red fluorescence located in the nuclei of Nup153-Cyt *c*-treated cells provides evidence of apoptosis, whereas DNA fragmentation is not evident in cells treated with vehicle alone (vehicle). Fixed and permeabilized cells were incubated with DNase I (3000 U/ml) to induce DNA strand breaks, prior to the labeling procedure and therefore acts as a positive control (DNase I). DNA fragmentation is comparable to cells treated with Nup153-Cyt *c*. As a negative control, fixed and permeabilized cells were treated with labeling solution without terminal deoxynucleotidyl transferase (-Tdt).

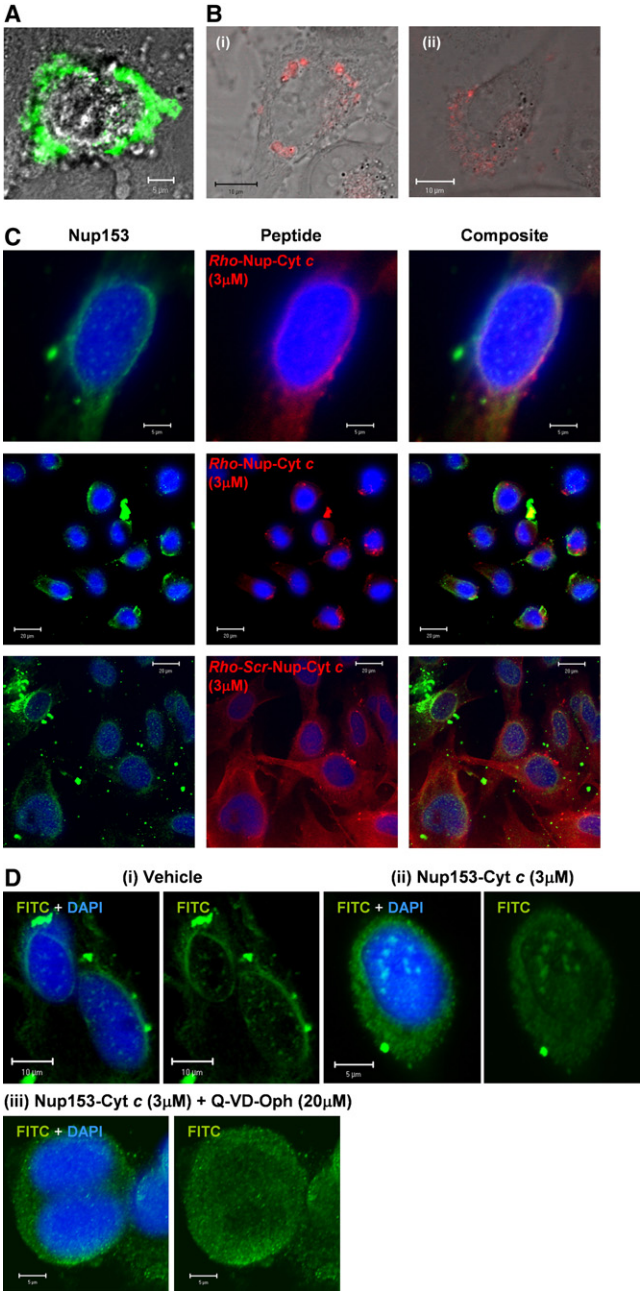

Figure 4. Nup153-Cyt *c*: Intracellular Distribution, Colocalization, and Redistribution of Nucleoporin 153

(A) Nup153 translocates to the nuclear periphery (early events). *Fluo*-Nup153$^{980–987}$ is liberated from *Fluo*-Nup153-M918 (Table 1) following cellular penetration and a subsequent intracellular reduction of cysteine. *Fluo*-Nup153$^{980–987}$ shown here in green now assumes a peripheral nuclear distribution. U373MG were treated with 5 μM *Fluo*-Nup153-M918 for 1 hr and visualized by live confocal cell imaging.

(B) U373MG cells were subsequently treated with either *Rho*-Nup153-Cyt *c* (3 μM) or the scrambled control peptide *Rho-scr*-Nup153-Cyt *c* (3 μM) and analyzed by live confocal cell imaging. After 45 min, *Rho*-Nup153-Cyt *c* assumed a predominant perinuclear distribution (i), whereas *Rho-scr*Nup153-Cyt *c* adopted a more generalized cytoplasmic distribution (ii). Cellular distributions of peptides for (A) and (B) are presented here merged with images taken under differential interference contrast microscopy and assist in highlighting the nucleus.

(C) Colocalization of *Rho*-Nup153-Cyt *c* with nucleoporin 153 (Nup153), (early events). U373MG cells were incubated for 45 min with *Rho*-Nup153-Cyt *c* (3 μM) or scrambled control. Fixed and permeabilized cells were immunostained for the nucleoporin protein Nup153 and viewed by confocal microscopy. Cells were counterstained with DAPI to visualize the nuclear DNA.

(D) Nup153-Cyt *c* elicits redistribution of Nup153 in U373MG cells (later events). Under control conditions, Nup153 resides in the nuclear periphery to face the nucleoplasm and can be visualized by predominant staining of the nuclear periphery (i). Following treatment with Nup153-Cyt *c*, Nup153 assumes a more diffuse pattern and redistributes to the nucleoplasm and cytoplasm (ii). U373MG cells were treated for 4 hr with Nup153-Cyt *c* (3 μM) or vehicle (medium alone). Treated cells were also coincubated with the pan-caspase inhibitor Q-VD-OPh (20 μM) (iii). Redistribution of Nup153 is still observed. Fixed cells were probed with primary (sheep polyclonal Anti-Nup153) and secondary (anti-sheep IgG conjugated to FITC) antibodies and visualized by confocal microscopy. Cells were counterstained with DAPI to visualize the nucleus.

receptors (IP_3R) located on the ER to amplify apoptotic-signaling events (Boehning et al., 2003).

DISCUSSION

Proteomimetic CPPs

A major aim of this study was to employ QSAR analysis of human Cyt *c* to identify cell penetrant sequences that can mimic the apoptogenic activity and trafficking events of the native protein. The distribution of highly probable CPPs within the Cyt *c* primary sequence was restricted to the closely paired N- and C-terminal helical domains that are a highly conserved structural motif. Two such sequences, Cyt *c*$^{77–101}$ and the shorter homolog Cyt *c*$^{86–101}$, translocate the plasma membrane to differentially accumulate in extranuclear (ER) or nuclear compartments, respectively. Moreover, these peptides also induce apoptosis in brain tumor cells, indicating that they mimic the role of Cyt *c* as a key regulator of apoptsis. Thus, these and other sequences contain both cell penetrating (*address*) and biologically active (*message*) pharmacophores that are discontinuously organized within a rhengnylogic peptide.

We also hypothesize that these helical sequences may constitute integral transduction or binding domains within Cyt *c* that enable the protein to interact with plasma, ER, and nuclear membranes. Moreover, the multifunctional roles of Cyt *c* require interaction with various biological membranes or targets. When released from mitochondria, cytosolic Cyt *c* not only triggers apoptosis by forming the apoptosome, a multimeric complex composed of Apaf-1 and caspase-9, but also accumulates within the nucleus to partake in chromatin remodelling (Nur-E-Kamal et al., 2004). Furthermore, cytosolic Cyt *c* binds to ER-located IP_3Rs to attenuate inositol 1,4,5-trisphosphate (IP_3)-mediated inhibition of calcium release (Boehning et al., 2003). Inhibition of this negative feedback drives a feed forward mechanism that sustains release of ER-derived calcium which in turn augments calcium accumulation within mitochondria with a consequential enhancement in mitochondrial membrane permeability and further release of Cyt *c*. Recent studies would also indicate that Cyt *c* internalizes into living cells (Howl and Jones, 2008), while the protein is also reported to play an extracellular role in inflammatory pathologies (Pullerits et al., 2005). Given the propensity of Cyt *c* to move from mitochondria to nucleus, ER, intracellular, and extracellular compartments, it is perhaps not surprising that

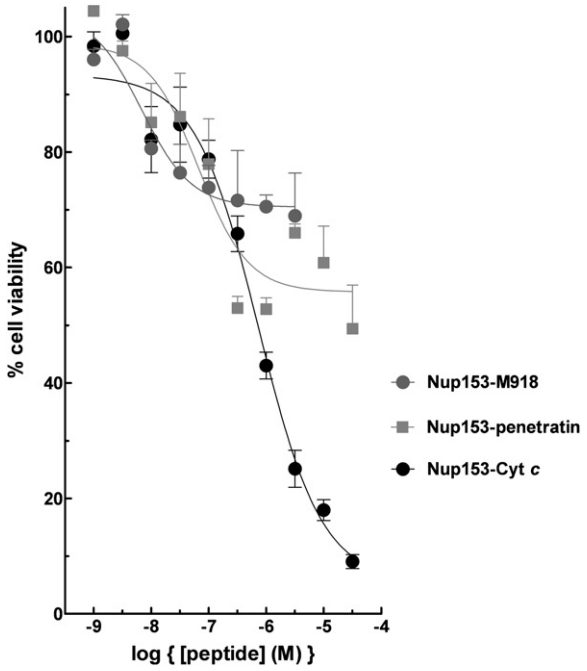

Figure 5. Intracellular Delivery of Nup153$^{980–987}$ Using Biologically Inert CPPs

U373MG cells were exposed to increasing concentrations of peptides (0.001–30 μM) for 24 hr. Cell viability was measured by MTT conversion and expressed as a percentage of those cells treated with vehicle (medium) alone. Data points are mean ± SEM from three experiments performed in sextruplicate.

proteomimetic CPP of Cyt *c* collectively target a similar range of organelles and milieu as discussed below.

Besides data presented herein, there are few yet growing reports of CPP prediction which have identified intrinsically biologically active CPP. QSAR analysis has identified CPP from the intracellular loops of G protein-coupled receptors that mimic the agonist-activated receptor. More specifically, a peptide derived from the C-terminal intracellular sequence of the rat angiotensin receptor (AT_{1a}) internalizes into living cells and elicits blood vessel contraction, while a peptide derived from the human glucagon-like peptide receptor (GLP-1R) induces insulin release from isolated pancreatic islets (Östlund et al., 2005). Similarly, we have identified a 20 amino acid cell penetrant fragment within the human type (a) calcitonin receptor ($hCTR_{(a)}$), $hCTR_{(a)174–193}$. Derived from the first intracellular loop, $hCTR_{(a)174–193}$ is an independent stimulator of CAMP formation and also demonstrates a direct activation of heterotrimeric G proteins, as was measured by the initial rate of binding of [^{35}S] GTPγS to rat brain cortical membranes (Jones et al., 2006). Though not originating from QSAR analysis, Johansson et al. (2008) have identified a cell permeable 22 amino acid peptide that corresponds to the N-terminal of p14ARF that inhibits the proliferative propensity of breast cancer cells. It is therefore most probable that CPP prediction will identify further cell penetrant proteomimetic peptides that can modulate key events in cell biology and pathology. Though we may not claim that such predictions are infallible (Hansen et al., 2008), QSAR-based analysis of probable CPP within signal transduction modulatory proteins is nevertheless a promising starting point.

Translocation Efficacies of Proteomimetic CPP

The peptide that demonstrated the greatest degree of cellular penetration was the comparative control peptide mitP (1455.8 ± 13.8-fold uptake). Accordingly, using both helical wheel predictions in secondary structure and hydropathicity indices, this peptide was predicted to be strongly amphipathic ($H\Phi$ = 0.49). However, a presumed amphipathic secondary structure can not purely account for enhanced cellular penetration since the hydropathicity value for penetratin ($H\Phi$ = −1.731) suggests a lesser degree of amphipathicity compared with all other Cyt *c*-derived peptides, yet penetratin displays a higher degree of cellular penetration (591.3 ± 37.52-fold uptake) (Figure 2). Similarly, the chimeric structures Nup153-Cyt *c* ($H\Phi$ = −0.336) and *scr*Nup153-Cyt *c* ($H\Phi$ = −0.336) and Cyt $c^{77–101}$ ($H\Phi$ = −0.317) alone present similar hydropathicity values and are thus predicted to share the same degree of amphipathicity. However, the chimeric structures Nup153-Cyt *c* (408.2 ± 15.58-fold uptake) and *scr*Nup153-Cyt *c* (412.5 ± 5.20-fold uptake) demonstrate an enhanced propensity for cellular penetration compared to Cyt $c^{77–101}$ (105.9 ± 0.42-fold uptake). It is therefore more likely that increased cationic charge provided by Lys^4 of the N-terminal extension Nup153$^{980–987}$ is accountable for this observation.

Nup153-Cyt *c*: Intracellular Targets and Biological Mechanisms of Action

Owing to its strong propensity for cellular penetration and moderate apoptogenic activity, Cyt $c^{77–101}$ was selected for further modification and development as a chimeric apoptogenic agent. Indeed, the apoptogenic potency of Cyt $c^{77–101}$ was most significantly enhanced by N-terminal extension with the peptide Nup153$^{980–987}$, a sequence derived from Nup153 and designed to target the NPC as a novel therapeutic strategy. Moreover, at earlier time points (45 min) *Rho*-Nup153-Cyt *c* assumes a predominant perinuclear distribution and more specifically, a strong colocalization with the protein Nup153. Suggested biological mechanisms underlying the apoptogenic potency of Nup153-Cyt *c* became more apparent following 4 hr of treatment with the peptide, principally, the diffuse redistribution of the NPC protein Nup153 from the nuclear periphery to the nucleoplasm and the cytoplasm. These data suggest that Nup153-Cyt *c* may modulate the control of nuclear transport events or indeed the functional utility of the NPC.

However, reduced cytotoxic potencies (moderate reductions in cellular viability) were observed following the intracellular delivery of Nup153$^{980–987}$ using either the inert CPP penetratin or M918. This observation coupled with a distinct perinuclear distribution of Nup153$^{980–987}$ when delivered into cells by M918 would indicate that Nup153-Cyt *c* targets additional intracellular compartments besides that of the nuclear pore complex in the orchestration of apoptotic events. It was initially postulated that the synergistic effect of Nup153-Cyt *c* may be attributable to this peptide chimera also interacting with IP_3Rs located within the ER. The following lines of evidence would support such a hypothesis (1) Cyt $c^{77–101}$ demonstrates a strong propensity for coloalization with ER (*coloc* coefficient = 0.996 ± 0.002) and (2) as mentioned previously, during early apoptotic events, the release of mitochondrial Cyt *c* modulates the function of IP_3Rs with a resultant augmentation in oscillatory calcium transients. This feed forward mechanism augments further Cyt *c* release

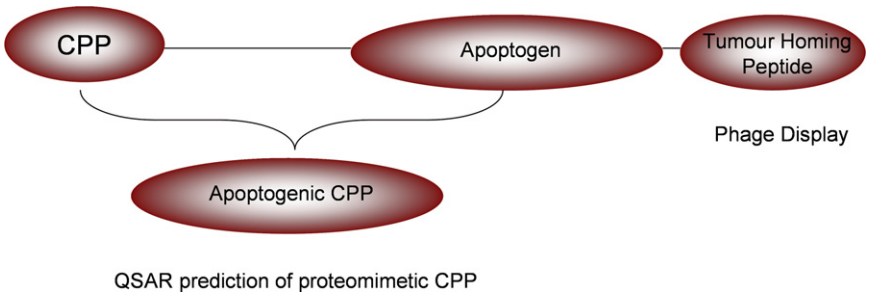

Figure 6. Modular Representation of Peptidyl Tumour Homing Constructs
CPP conjugation enhances the bioavailabilty of apoptogenic moities (Myrberg et al., 2008) and inclusion of THPs ensures a directed specific targeting to tumor cells, their vasculature, or lympahtics (Enbäck and Laakkonen, 2007). However, somewhat difficult conjugation steps between CPPs and apoptogenic pharmacotherapeutics can be circumvented by the use of apoptogenic CPPs which possess the dual features of cellular penetration and biological activity.

to amplify the apoptotic signal (Boehning et al., 2003). Most notably, the region of the IP_3R to which Cyt *c* binds is dependent upon a cluster of glutamic acid residues within the C-terminal of the channel (Boehning et al., 2005). It is thus not implausible that the highly basic Cyt $c^{77–101}$ peptide encompasses the interaction domain which coordinates Cyt *c* binding to IP_3Rs through electrostatic interactions. However, while this mechanism could account for the moderately apoptogenic features of Cyt $c^{77–101}$ alone, data presented herein indicate a poor colocalization of the chimeric construct Nup153-Cyt *c* with ER (*coloc* coefficient = 0.287 ± 0.065) and emphasize a strong colocalization with Nup153 (*coloc* coefficient = 0.93 ± 0.024).

Moreover, and as previously alluded to, the multifunctional roles of Cyt *c* require the protein to translocate numerous biological membranes including the cytoplasmic-nuclear interface. Cyt *c* translocates to the nucleus to partake in chromatin remodeling (Nur-E-Kamal et al., 2004) and apoptotic cells show perinuclear Cyt *c* aggregation (Ruiz-Vela et al., 2002). Thus, Cyt $c^{77–101}$ may very well posses a nuclear translocation sequence/integral transduction domain, which may facilitate the targeting /incorporation of Nup153-Cyt *c* to the NPC.

It is noteworthy that the apoptogenic features of Cyt $c^{77–101}$ are not likely to be attributable to apoptosome formation since Cyt $c^{77–101}$ does not encompass the domain/amino acids required for apoptosome activation. Notably, alanine substitution of Lys^{72} of Cyt *c* fails to oligomerize with Apaf-1 (Hao et al., 2005). Furthermore, unpublished data from studies using isolated mitochondria demonstrate that Cyt $c^{77–101}$ fails to elicit mitochondrial matrix swelling and permeabilisation of inner mitochondrial membranes. Thus, the apoptogenic mechanism employed by Cyt $c^{77–101}$ is unlikely to necessitate direct release of endogenous mitochondrial Cyt *c*.

Endosomal entrapment with a consequential reduction in biological efficacy is in some cases, problematic when utilizing CPP for intracellular cargo delivery. This phenomenon largely depends upon the specific CPP and/or the cargo of interest and is therefore by no means predictable (Räägel et al., 2009). Accordingly, the high potency exhibited by Nup153-Cyt *c* may be attributable in part to the presented proteomimetic Cyt *c* peptides escaping endosomal entrapment, as is demonstrated by their ability to specifically accumulate at distinct intracellular localizations.

Utility of Apoptogenic CPP and the Cell-Specific Induction of Apoptosis

Nup153-Cyt *c* demonstrates potential as a potent inducer of apoptosis. Moreover, unlike extensively processed apotogenic pharmaceuticals where every potential modification site is a pharmacophore, CPPs more easily afford the incorporation of *homing* peptides. Thus, the inclusion of *homing* sequences which recognize markers expressed or overexpressed on tumor cells could ensure a directed therapeutic induction of apoptosis while sparing healthy tissue. Such tumor homing peptide (THP) sequences are now being identified through phage display technologies (Enbäck and Laakkonen, 2007) and can be part of a modular framework for the design of tumor-specific apoptogenic constructs as presented below (Figure 6).

SIGNIFICANCE

The molecular properties of the two Cyt *c*-derived peptides, Cyt $c^{77–101}$ and Cyt $c^{86–101}$, peptides that are both cell penetrating and apoptogenic clearly demonstrate that the prediction of CPP can also identify rhegnylogically organized proteomimetics. Furthermore, the novel chimeric construct Nup153-Cyt *c*, derived by N-terminal extension of Cyt $c^{77–101}$, demonstrates potential as a potent inducer of apoptosis and further propounds the nuclear pore complex as a novel target for the therapeutic induction of apoptosis. Moreover, while CPP are emerging as promising candidates for future drug delivery, owing to their ability to improve cellular uptake, thus enhancing bioavailability, CPP with specific biological activity carry the additional bonus of simplifying often complex conjugation steps. Indeed, proteomimetic CPP may easily be incorporated into constructs with peptidyl *address* motifs, the latter of which could enhance the selectivity of drug delivery leading to a probable reduction in nonselective side effects.

EXPERIMENTAL PROCEDURES

Prediction of CPP

As previously described (Hällbrink et al., 2005), QSAR analyses can be used to identify putative CPPs within the primary sequence of proteins. We employed this method to assess the averaged bulk property values of amino acids within a sequence of Cyt *c* (5–30 amino acids in length) and compared these with defined values obtained from a training set of 24 CPP and 17 nonpenetrant analogs.

Peptide Synthesis, Purification, and Analysis

A majority of the peptides utilized in this study were manually synthesized (0.1–0.2 mmol scale) on Rink amide methylbenzhydrylamine (MBHA) resin (Novabiochem, Beeston, UK) employing an N-α-Fmoc protection strategy with O-Benzotriazole-N,N,N',N'-tetramethyl-uronium-hexafluoro-phosphate (HBTU, Novabiochem)) or O-(6-Chloro-1-hydrocibenzotriazol-1-yl)- 1,1,3,3-tetramethyluronium hexafluorophosphate (HCTU; AGTC Bioproducts, Hessle,

UK) activation. The cell penetrating vector M918 (*H*-MVTVLFRRLRIRRA CGPPRVRV-NH_2) and the cargo *H*-CNFKFGLSSK($N^{\varepsilon\text{-}5,6\text{-carboxy-flourescein}}$)-$NH_2$ (*fluor*Nup153) (Table 1) were synthesized on an Applied Biosystems model 433A synthesizer using *t*-Boc chemistry as recently reported (El-Andaloussi et al., 2007). To facilitate conjugation, equimolar amounts of M918 with an amino-terminal Cys(3-nitro-2-pyridinesulfanyl) and *H*-CNF KFGLSSK(N^{ε}-5,6-carboxy-flourescein)-NH_2 were solvated in a mixture of 250 μl dimethylformamide (DMF) and 250 μl 50 mM acetic acid buffer (pH 5.0). The solution was purged with N_2 for 4 min followed by 4 hr incubation while mixing the contents continuously.

All other fluorescent peptides, to be used in confocal live cell imaging and quantitative uptake analyses, were synthesized by amino-terminal acylation of CPP sequences with 6-carboxy-tetramethylrhodamine (Novabiochem, Beeston, UK) as reported previously (Jones et al., 2008). Crude peptides were purified to apparent homogeneity by semipreparative scale high-performance liquid chromatography (Jones et al., 2008; El-Andaloussi et al., 2007). The predicted masses of all peptides used (average $M + H^+$) were confirmed to an accuracy of ± 1 by matrix-assisted laser desorption ionization (MALDI) time of flight MS operated in positive ion mode using α-cyano-4-hydroxycinnamic acid (Sigma) as a matrix.

Cell Culture

U373MG human astrocytoma cells were routinely maintained in a humidified atmosphere of 5% CO_2 at 37°C in DMEM supplemented with L-glutamine (0.1 mg/ml) 10% (w/v) fetal bovine serum (FBS), penicillin (100 U/ml), and streptomycin (100 μg/ml).

Quantitative Analyses of Peptide Translocation

U373MG cells were cultured as above, transferred to 25 cm^2 tissue culture flasks and grown to 75% confluence. Immediately prior to the addition of fluorescent peptides, cells were washed with and transferred into 2 ml of stimulation medium (SM; DMEM without phenol red). Cells were incubated with fluorescent peptides at a final concentration of 5 μM for 1 hr in SM at 37°C in a humidified atmosphere of 5% CO_2. Cells were then washed once in Hanks Balance Salt Solution, three times SM, and detached with 400 μl of 1% trypsin at 37°C. Cells were collected by centrifugation from 800 μl of SM and pellets lysed in 450 μl 0.1 M NaOH for 2 hr on ice. Samples (200 μl) of cell lysates were mixed with 300 μl of 0.1 M NaOH, transferred to a 1 ml quartz cuvette, and analyzed using a Hitachi F-2500 fluorescence spectrophotometer (λAbs 552nm/λEm 580 nm).

Confocal microscopy

Live Cell Imaging Analysis

U373MG cells were transferred to 35 mm sterile glass base dishes (IWAKI, Japan) and grown to 75% confluence (conditions as described above). Immediately prior to the addition of fluorescent peptides and/or other materials, cells were washed with and transferred into SM. During the period of exposure to peptides, cell layers were maintained at 37°C in a humidified atmosphere of 5% CO_2. Immediately prior to observation, cells were then washed gently with SM (8×) and analyzed with a Carl Zeiss LSM510Meta confocal microscope equipped with a live cell imaging chamber.

Quantitative Colocalization

For ER colocalization studies, cells were incubated with 1 μM ERTracker® Green FM (Molecular Probes, Invitrogen, Paisley, UK) alongside fluorescent peptides and viewed by live confocal cell imaging. For Nup153 colocalization studies, U373MG cells were grown to 75% confluence on coverslips in six-well plates, washed, and treated with 3 μM peptides for 45 min. Cells were washed with phosphate-buffered saline (PBS; pH 7.4) and fixed with cold methanol:acetone (1:1, v/v) for 10 min on ice. To remove fixative cells were washed x 3 in PBS, then blocked with 1% (v/v) FBS in PBS for 30 min at room temperature. Washed cells were allowed to air dry and then were incubated with primary sheep anti-human, anti-Nup153 antibody (ImmuQuest) for 1 hr at room temperature in the dark. Cells were washed five times with PBS and incubated with secondary antibody (1:100), rabbit anti-sheep IgG conjugated to FITC (Sigma) for a further 1 hr at room temperature in the dark. Coverslips were washed in PBS, air-dried, and mounted on slides with Vectashield (Vector Laboratories Inc., Peterborough, UK) containing 4′6′ diamidino-8-phenylindole dihydrochloride (DAPI) to counterstain double-stranded DNA.

Quantitative colocalization was performed using the Carl Zeiss quantitative colocalization analysis software, incorporating an interactive scatter plot and data table linked to the images. Pixels showing an intensity above the background of both channels (background defined as, pixels in channel 1 only, e.g., rhodamine and pixels in channel 2 only, e.g., fluorescein) were designated as colocalized pixels. Data were collected from an average of 12 regions of interest, between 50 and 200 μm^2 and from three independent experiments. Colocalization (coloc) coefficients were calculated for the two different fluorophores according to the following equations: C1 = pixels channel 1 coloc/pixels channel 1 total, C2 = pixels channel 2 coloc/pixels channel 2 total and defined as relative number of colocalizing pixels in channel 1(designated rhodamine) or 2 (designated fluorescein), respectively, as compared with the total number of pixels above threshold. Coefficients generated values between 0 and 1. A value of 0 indicated no colocalization, whereas a value of 1 indicated that all pixels were colocalized.

Redistribution of Nup153

U373MG cells were grown to 75% confluence on coverslips in six-well plates, washed, and treated with 3 μM Nup153-Cyt *c* (3 μM) or vehicle (medium) alone for 4 hr. Fixation and immunostaining with anti-Nup153 antibody (ImmuQuest) and IgG conjugated to FITC (Sigma) were carried out as above and cells were viewed under confocal microscopy. When required, Nup153-Cyt *c*-treated cells were coincubated with the pan-caspase inhibitor Q-VD-OPh, Non-O-methylated (20 μM) (Calbiochem, Merck) for 4 hr.

MTT Conversion Assay

Peptide-induced changes in cellular viability were quantitatively assessed using the 3-(4,5-dimethylthazol-2-yl)-2,5-diphenyl tetrazolium bromide (MTT) conversion assay (Jones et al., 2008; Carmichael et al., 1987). U373MG cells were cultured as above in 96-well plates, treated with peptides for 24 hr at 37°C, and further incubated with MTT (0.5 mg/ml) for 3 hr at 37°C. The insoluble formazan product was solubilized with DMSO and MTT conversion determined by colorimetric analysis at 540 nm. Cellular viability was expressed as a percentage of those cells treated with vehicle (medium) alone. Graphical representations of changes in cell viability were calculated using GraphPad Prism 5 software.

Tunel Assay

Nuclear DNA fragmentation, a characteristic of apoptosis, was detected by the Tdt (terminal deoxynucleotidyl transferase)-mediated dUTP nick end labeling (TUNEL) assay according to manufacturer's instructions (In Situ Cell Death Detection kit, TMR red, Roche, UK). U373MG cells were grown to 75% confluence on coverslips in six-well plates, washed, and treated with peptides or vehicle alone (medium) for 18 hr. Cells were washed with phosphate-buffered saline (PBS; pH 7.4) and fixed with 4% (w/v) formaldehyde in PBS for 1 hr at room temperature. Fixed cells were permeabilized with 0.1% (v/v) Triton X-100 in 0.1% (w/v) sodium citrate at 4°C for 2 min and then incubated for 1 hr at 37°C in a humidified atmosphere in the dark with TUNEL reaction mixture containing Tdt and TMR red-dUTP to label free 3′OH ends in the DNA. Coverslips were washed in PBS, air-dried, and mounted on slides with Vectashield (Vector Laboratories Inc., Peterborough, UK) containing 4′6′ diamidino-8-phenylindole dihydrochloride (DAPI) to counterstain double-stranded DNA in the nuclei. Positive controls were achieved by incubating fixed and permeabilized cells with DNase I, grade 1 (3000 U/ml in 50 mM Tris-HCl [pH 7.5], 1 mg/ml BSA) for 10 min at room temperature to induced DNA strand breaks, prior to the labeling procedure. Negative controls were achieved by incubating fixed and permeabilized cells in TUNEL reaction mixture without Tdt. Samples were analyzed using a Carl Zeiss LSM 510 Meta confocal microscope.

Caspase-3 Activation

Detection of caspase-3 activity was measured using the DEVD-NucView 488 caspase-3 substrate (Biotium Inc., Cambridge Bioscience, Cambridge, UK) according to manufacturer's instructions. U373MG cells were grown to 75% confluence in 35 mm sterile glass base dishes (IWAKI) and treated with peptides or vehicle alone for 4 hr at 37°C. Thereafter, DEVD-NucView 488 caspase-3 substrate was added at a final concentration of 5 μM for a further 30 min. As an additional control, treated cells were incubated with the caspase-3 inhibitor Ac-DEVD-CHO (25 μM), 30 min prior to substrate addition.

Nuclear staining and fluorescence was observed using a Carl Zeiss LSM 510 Meta confocal microscope.

ACKNOWLEDGMENTS

This work was funded in part by the Samantha Dickson Brain Tumour Trust. Studies were also supported by Swedish Research Council (VR-NT); by Center for Biomembrane Research, Stockholm; by Knut and Alice Wallenberg's Foundation; by the EU through the European Regional Development Fund through the Center of Excellence in Chemical Biology, Estonia; by the targeted financing SF0180027s08 from the Estonian Government; by the DoRa Program of The European Social Fund; and by Archimedes Foundation.

Received: February 15, 2010
Revised: April 29, 2010
Accepted: May 19, 2010
Published: July 29, 2010

REFERENCES

Arnt, C.R., Chiorean, M.V., Heldebrant, M.P., Gores, G.J., and Kaufmann, S.H. (2002). Synthetic Smac/DIABLO peptides enhance the effects of chemotherapeutic agents by binding XIAP and cIAP1 in situ. J. Biol. Chem. *277*, 44236–44243.

Bednenko, J., Cingolan, G., and Gerace, L. (2003). Nucleocytoplasmic transport: navigating the channel. Traffic *4*, 127–135.

Boehning, D., Patterson, R.L., Sedaghat, L., Glebova, N.O., Kurosaki, T., and Snyder, S.H. (2003). Cytochrome *c* binds to inositol (1,4,5) trisphosphate receptors, amplifying calcium-dependent apoptosis. Nat. Cell Biol. *5*, 1051–1061.

Boehning, D., Van Rossum, D.B., Patterson, R.L., and Snyder, S.H. (2005). A peptide inhibitor of cytochrome *c*/inositol 1,4,5-trisphosphate receptor binding blocks intrinsic and extrinsic cell death pathways. Proc. Natl. Acad. Sci. USA *102*, 1466–1471.

Carmichael, J., DeGraff, W.G., Gazdar, A.F., Minna, J.D., and Mitchell, J.B. (1987). Evaluation of a tetrazolium-based semiautomated colorimetric assay: assessment of chemosensitivity testing. Cancer Res. *47*, 936–942.

Derossi, D., Joliot, A.H., Chassaing, G., and Prochiantz, A. (1994). The third helix of the Antennapedia homeodomain translocates through biologial membranes. J. Biol. Chem. *269*, 10444–10450.

El-Andaloussi, S., Johansson, H.J., Holm, T., and Langel, Ü. (2007). A novel cell-penetrating peptide, M918, for efficient delivery of proteins and peptide nucleic acids. Mol. Ther. *15*, 1820–1826.

Enbäck, J., and Laakkonen, P. (2007). Tumour-homing peptides: tools for targeting, imaging and destruction. Biochem. Soc. Trans. *35*, 780–783.

Fulda, S., Wick, W., Weller, M., and Debatin, K.M. (2002). Smac agonists sensitize for Apo2L/TRAIL- or anticancer drug-induced apoptosis and induce regression of malignant glioma *in vivo*. Nat. Med. *8*, 808–815.

Hällbrink, M., Kilk, K., Elmquist, A., Lundberg, P., Lindgren, M., Jiang, Y., Pooga, M., Soomets, U., and Langel, Ü. (2005). Prediction of cell-penetrating peptides. Int. J. Pept. Res. Ther. *11*, 249–259.

Hansen, M., Kilk, K., and Langel, Ü. (2008). Predicting cell-penetrating peptides. Adv. Drug Deliv. Rev. *60*, 572–579.

Hao, Z., Duncan, G.S., Chang, C., Elia, A., Fang, M., Wakeham, A., Okada, H., Calzascia, T., Jang, Y., You-Ten, A., et al. (2005). Specific ablation of the apoptotic functions of cytochrome c reveals a differential requirement for cytochrome c and Apaf-1 in apoptosis. Cell *121*, 579–591.

Howl, J., and Jones, S. (2008). Proteomimetic cell penetrating peptides. Int. J. Pept. Res. Ther. *14*, 359–366.

Howl, J., Jones, S., and Farquhar, M. (2003). Intracellular delivery of bioactive peptides to RBL-2H3 cells induces β-hexoseaminidase secretion and phospholipase D activation. Chembiochem *4*, 1312–1316.

Jiang, X., and Wang, X. (2004). Cytochrome *c*-mediated apoptosis. Annu. Rev. Biochem. *73*, 87–106.

Johansson, H.J., El-Andaloussi, S., Holm, T., Mäe, M., Janes, J., Maimets, T., and Langel, Ü. (2008). Characterization of a novel cytotoxic cell-penetrating peptide derived from p14ARF protein. Mol. Ther. *16*, 115–123.

Jones, S., Farquhar, M., Martin, A., and Howl, J. (2005). Intracellular translocation of the decapeptide carboxyl terminal of $G_i3\alpha$ induces the dual phosphorylation of p42/p44 MAP kinases. Biochim. Biophys. Acta *1745*, 207–214.

Jones, S., and Howl, J. (2004). Charge delocalisation and the design of novel mastoparan analogues: enhanced cytotoxicity and secretory efficacy of [Lys^5, Lys^8, Aib^{10}]MP. Regul. Pept. *121*, 121–128.

Jones, S., Martel, C., Belzacq-Casagrande, A., Brenner, C., and Howl, J. (2008). Mitoparan and target-selective chimeric analogues: membrane translocation and intracellular redistribution induces mitochondrial apoptosis. Biochim. Biophys. Acta *1783*, 849–863.

Jones, S., Östlund, P., Langel, Ü., Zorko, M., Nicholl, I., and Howl, J. (2006). A rhegnylogic strategy for the synthesis of signal transduction modulatory, cell penetrating peptides. J. Pept. Sci. *12*, 92–92.

Langel, Ü. (2007). Handbook of Cell-Penetrating Peptides, Second Edition (Boca Raton, FL: CRC Press).

Lindgren, M., Hällbrink, M., Prochiantz, A., and Langel, Ü. (2000). Cell-penetrating peptides. Trends Pharmacol. Sci. *21*, 99–103.

Myrberg, H., Zhang, L., Mäe, M., and Langel, Ü. (2008). Design of a tumor-homing cell-penetrating peptide. Bioconjug. Chem. *19*, 70–75.

Nur-E-Kamal, A., Gross, S.R., Pan, Z., Balklava, Z., Ma, J., and Liu, L.F. (2004). Nuclear translocation of cytochrome *c* during apoptosis. J. Biol. Chem. *279*, 24911–24914.

Östlund, P., Kilk, K., Lindgren, M., Hällbrink, M., Jiang, Y., Budihna, M., Cerne, K., Bavec, A., Östenson, C.G., Zorko, M., and Langel, Ü. (2005). Cell-penetrating mimics of agonist-activated G-Protein coupled receptors. Int. J. Pept. Res. Ther. *11*, 237–247.

Portoghese, P.S. (1989). Bivalent ligands and the message-address concept in the design of selective opioid receptor antagonists. Trends Pharmacol. Sci. *10*, 230–235.

Prunuske, A.J., Liu, J., Elgort, S., Joseph, J., Dasso, M., and Ullman, K.S. (2006). Nuclear envelope breakdown is coordinated by both Nup358/RanBP2 and Nup153, two nucleoporins with zinc finger modules. Mol. Biol. Cell *17*, 760–769.

Pullerits, R., Bokarewa, M., Jonsson, I.-M., Verdrengh, J.M., and Tarkowski, A. (2005). Extracellular cytochrome *c*, a mitochondrial apoptosis-releted protein, induces arthritis. Rheumatology *44*, 32–39.

Räägel, H., Säälik, P., Hansen, M., Langel, Ü., and Pooga, M. (2009). CPP-protein constructs induce a population of non-acidic vesicles during trafficking through endo-lysosomal pathway. J. Control. Release *139*, 108–117.

Ruiz-Vela, A., De Buitrago, G.G., and Martinez-A, C. (2002). Nuclear Apaf-1 and cytochrome *c* redistribution following stress-induced apoptosis. FEBS Lett. *517*, 133–138.

Schwarze, S., and Dowdy, S.F. (2000). *In vivo* protein transduction: intracellular delivery of biologically active proteins, compounds and DNA. Trends Pharmacol. Sci. *21*, 45–48.

Snyder, E.L., Meade, B.R., Saenz, C.C., and Dowdy, S.F. (2004). Treatment of terminal peritoneal carcinomatosis by a transducible p53-activating peptide. PLoS Biol. *2*, e36. 10.1371/journal.pbio.0020036.

Tseng, Y.-L., Liu, J.-J., and Hong, R.-L. (2002). Translocation of liposomes into cancer cells by cell-penetrating peptides penetratin and Tat: A kinetic and efficacy study. Mol. Pharmacol. *62*, 864–872.

Walther, T.C., Fornerod, M., Pickersgill, H., Goldberg, M., Allen, T.D., and Mattaj, I.W. (2001). The nucleoporin Nup153 is required for nuclear pore basket formation, nuclear pore complex anchoring and import of a subset of nuclear proteins. EMBO J. *20*, 5703–5714.

